

International Journal of Modern Physics D  
© World Scientific Publishing Company

## Critical mass, moment of inertia and universal relations of rapidly rotating neutron stars with exotic matter

Smruti Smita Lenka

*BITS Pilani, Hyderabad Campus, Shameerpet Mondal, Hyderabad 500078, India*

Prasanta Char

*Inter-University Centre for Astronomy and Astrophysics, Post Bag-4, Ganeshkhind, Pune, India*

Sarmistha Banik \*

*BITS Pilani, Hyderabad Campus, Shameerpet Mondal, Hyderabad 500078, India*

Received 30 January 2017

Revised 21 April 2017

We calculate moment of inertia of neutron star with different exotic constituents such as hyperons and (anti)kaon condensates and study its variation with mass and spin frequency. The sets of equation of state, generated within the framework of relativistic mean field model with density-dependent couplings are adopted for the purpose. We follow the quasi-stationary evolution of rotating stars along the constant rest mass sequences, that varies considerably with different constituents in the equation of state. We also explore the universal relations associated with some of the normalised properties, such as critical mass and moment of inertia for specific EoS or as a matter of fact constituents of the dense matter. Deviations in the universal relations for moment of inertia are observed at higher compactness. This study presents important results concerning the properties of neutron stars, that could be observationally verified in the near future using Square Kilometer Array telescope.

*Keywords:* neutron stars, rotation, hyperon, antikaon condensates

97.10.Nf, 97.10.Pg, 97.10.Kc, 26.60.Kp

### 1. Introduction

Out of estimated total galactic population of a few tens of thousands of pulsars beaming towards the earth, we observe  $\sim 2500$  radio pulsars in our galaxy so far.<sup>1</sup> Among these known sources, fewer than 10% are in binary systems and only their mass could be measured precisely using Shapiro delay or a combination of post-Keplerian orbital parameters such as orbital period decay, advance of periastron, and constraints from spectroscopic modeling of the companion star.<sup>2</sup> The best studied

---

\*sarmistha.banik@hyderabad.bits-pilani.ac.in

pulsars in the neutron star binaries are the Hulse-Taylor pulsar, J0737-3039 etc. Masses are determined not only for double neutron star systems, but for several neutron star-white dwarf binaries as well, since they allow measurement of orbital period decay. Mass of accreting neutron stars can also be constrained by measuring the motion and spectral properties of the companions, but this process has large uncertainties.

Besides mass the other important observable of the neutron star is radius. There are several methods to constrain the radius utilising various properties of thermonuclear bursts, accretion-powered millisecond pulsars, kHz QPOs, relativistic broadening of iron lines, quiescent emissions, and binary orbital motions, but they are not free from systematic uncertainties.<sup>3</sup> Independent mass and radius measurement for the same compact star without invoking their combination, for example redshift, is yet to happen due to various uncertainties such as the estimated distance of the source, the unknown chemical compositions of the atmosphere, interstellar absorption, and the presence of magnetic field.<sup>4</sup>

Such astronomical techniques of mass-radius measurement should be complemented with theoretical investigations to get a complete picture of a neutron star. Observationally we can not directly probe the deep interior of a neutron star. There are several microscopic models that theoretically compute the equation of state (EoS) i.e. pressure( $P$ ) and energy density( $\epsilon$ ) at a certain density for the degenerate matter. Hence for a given EoS the static mass-radius relationship is generated by solving the Tolman-Oppenheimer-Volkoff (TOV) equation. For a rotating star also, this mass-radius sequence can be generated upto its maximum rotation frequency i.e. Kepler frequency. The set of EoS that does not conform to the latest mass measurement<sup>5-7</sup> is ruled out. However, it is equally important to constrain the EoS with the simultaneous observation of radius. And we lack reliable data of radius, as has already been mentioned. After the discovery of highly relativistic binary systems such as the double pulsar system PSR J0737-3039 for which masses of both pulsars are known accurately, it was argued that a precise measurement of moment of inertia ( $I$ ) of one pulsar might overcome the uncertainties in the determination of radius ( $R$ ) since dimensionally  $I \propto MR^2$ .<sup>4</sup> In relativistic binary systems, higher order post Newtonian (PN) effects could be measured. Furthermore, the relativistic spin-orbit (SO) coupling may manifest in an extra advancement of periastron above the PN contributions such that the total advance of periastron is  $\dot{\omega} = \dot{\omega}_{1PN} + \dot{\omega}_{2PN} + \dot{\omega}_{SO}$ .<sup>8</sup> The SO contribution has a small effect and could be measured when it is comparable to the 2PN contribution. The measurement of the SO effect leads to the determination of moment of inertia ( $I$ ) of a pulsar in the double pulsar system.<sup>2,9</sup> However simulations assuming  $5\mu s$  timing precision for the pulsar A of PSR J0737-3039 predict that it would take another 20 years to measure  $I$  at 10% accuracy.<sup>10</sup>

This situation would change vastly with the advent of world's largest radio telescope, the Square Kilometer Array (SKA), which is expected to begin operations early in the next decade. The high precision timing technique in the SKA would quicken the determination of the moment of inertia of the double pulsar PSRJ0737-

3039A. The distinguishable effect of pulsar moment of inertia on the pulsar timing in SKA will be of the order of the 2PN level correction to the advance of periastron  $\dot{\omega}$ , due to highly improved precision of timing measurements over its predecessors. It can also measure  $\mathbf{I}$  by estimating the spin-orbit misalignment angle  $\delta$  in double neutron stars. SKA can potentially discover highly relativistic binaries, exotic system like pulsar-black hole binary and sub-millisecond pulsar.<sup>2</sup> Simultaneous measurement of high mass and high spin stars would be particularly helpful in constraining the mass-radius relation. Also, the mass-radius profiles from different models can intersect among themselves. Therefore, we need a third independent parameter to constrain the EoS, i.e. spin, which is the first measured quantity. So, at least three independent global parameters, for example, mass, radius and spin frequency, of the same star are required in order to constrain the EoS models, and hence to understand the dense core.<sup>3</sup> Moreover, the spin off from the measurement of  $\mathbf{I}$  in the SKA looks promising. The first consequence is the estimation of radius in highly relativistic binaries where mass of each neutron star is accurately determined. Secondly, if the back bending effect is observed, it might reveal a phase transition from nuclear matter to some exotic form of matter (hyperon or quark) in neutron star interior.<sup>11</sup> Furthermore, moment of inertia measurement would also shed light on the I-Love-Q relation. Masses, radii, backbending and stability for rotating neutron stars with hyperon and quark cores are discussed in Ref.<sup>11</sup> Backbending was also reported for rotating neutron stars with quark core in Ref.<sup>12,13</sup> We neglect all the secular instabilities that may appear at very high rotation. These instabilities decay by emitting gravitational radiation, reducing the speed of the stars in realistic cases before attaining the Kepler limit. But we have not considered this in the spin down.

If the moment of inertia is measured with 10% uncertainty, this would constrain the radius of a  $1.4M_{\odot}$  star with 6% – 7% uncertainty.<sup>4</sup> But again, there will be a family of EoS models in  $\mathbf{I}$ -M curve lying in that range. Thus, it is crucial to examine the dependence of  $\mathbf{I}$  on EoS. As of now there are several EoS models available for neutron star core. We are yet to reach a consensus on the compact star EoS, due to our limited knowledge of the nature of matter beyond normal nuclear matter density. Neutron star matter should encompass a wide range of densities; from the density of iron nucleus at the surface of the star to several times normal nuclear matter density in the core. At this high density interior of neutron stars, the chemical potentials of nucleons and leptons increase rapidly. Consequently several novel phases with large strangeness fraction such as, hyperon matter, Bose-Einstein condensates of strange mesons and quark matter may exist. The presence of exotic matter typically softens the EoS, resulting in a smaller maximum mass neutron star than that of the nuclear EoS.<sup>14</sup> So, does the deep interior of a neutron star really contain the strangeness degrees of freedom? Comparing the values of mass-radius obtained using the astronomical techniques along with the theoretical predictions may solve the long-standing puzzle. Currently the accurately measured high-mass neutron stars are PSRs J1614-2230 and J0348+0432 with masses  $1.928 \pm 0.017$  and  $2.01 \pm 0.04 M_{\text{Solar}}$  respectively.<sup>5-7</sup> They put a strong constraint on the EoS of neutron

star matter and rule out most of the soft EoS only from the mass measurement.

In recent years, there has also been an alternative approach to this puzzle, namely the study of universal relations among several quantities that characterizes a compact object. These relations are supposed to be independent of the EoS of the star. Therefore if one of them is measured, the other can be estimated from an analytical expression without taking into consideration the internal structure of the star. It has been discovered that such relations exist among the moment of inertia ( $\mathbf{I}$ ), the Love number associated with the tidal deformation and spin induced quadrupole moment ( $Q$ ).<sup>15,16</sup> But, many of these universality relations are approximate as they exist only in some particular regime such as slow rotation approximation and not very strong magnetic field. It has been shown that at very high rotational frequencies the universality between  $\mathbf{I}$  and  $Q$  breaks down as both the deviations due to EoS and spin frequency are comparable at high spin frequency.<sup>17</sup> It has also been shown that a comparatively slowly rotating star ( $P \gtrsim 10s$ ) and strong magnetic fields ( $B \gtrsim 10^{12}G$ ), the universality between  $\mathbf{I}$  and  $Q$  breaks down.<sup>18</sup> The slowly rotating stars are found to abide by universal relations as reported in Refs.<sup>15,16</sup> Many authors tried to highlight a relation between normalised moment of inertia ( $\mathbf{I}/MR^2$ ) and stellar compactness( $M/R$ ).<sup>4,17,19-22</sup> Also, having a universal relation will allow us to determine the radius with a very high accuracy once we have simultaneous measurements of  $\mathbf{I}$  and mass of the same star.

Recently, Breu and Rezzolla<sup>21</sup> have studied such universal relations in great detail. They have also used another normalisation for moment of inertia as ( $\mathbf{I}/M^3$ ) and showed that universality relation holds more tightly than the previous case. In their analysis, they have taken a large set of EoS with different stiffness. However, the matter they considered is nucleonic. They satisfy the two solar mass limit, but many of them use non-relativistic interactions, and some of the relativistic EoS also use the parameter sets that are not favorable in view of the symmetry energy nuclear experimental data. It is not known if the inclusion of exotic components or a phase transition inside the neutron star core would effect the universality relations. This is one of the main goals of the present work. We are also motivated to study the effect of higher rotational frequencies on the universality relation between normalized moment of inertia and stellar compactness.

Here in this paper, we consider different compositions in our EoS which is generated under the framework of density dependent relativistic mean field model<sup>23,24</sup> and study the variation of mass-radius profile for different EoS and how they evolve with uniform rotation of the neutron stars. We also study the maximum mass sustainable for rotating configuration, expressed in terms of dimensionless and normalised angular momenta. Next, we follow the variation of  $\mathbf{I}$  with gravitational mass and observe how rotation affects  $\mathbf{I}$  for different constituents of dense matter relevant to the neutron star core. Finally, we investigate if there exists a universal relations between  $\mathbf{I}$  and compactness ( $M/R$ ). We use two types of normalised moment of inertia relations prescribed by Ref<sup>4,21</sup> for EoS with nucleon, hyperon and antikaon condensates degrees of freedom for rapidly rotating compact stars.

The paper is organised as follows. In Section II, we briefly discuss the rotating neutron stars, the rns code that we use to generate our results and EoS. Section III is devoted to results and discussion. Finally we summarise in Section IV.

## 2. Rotating neutron stars and EoS

Pulsars are rotating neutron stars with a strong magnetic field. Their magnetic axes are not aligned to their rotation axes and the continuous radio emission from the magnetic poles sweeps our line of sight periodically. Observations convey that the time period of pulsars vary from approximately 1 ms to 10 seconds.<sup>1</sup> Most of the pulsars discovered so far, take nearly 1 sec to complete one revolution. The slowest one, observed in 2011, takes an exceptionally large amount of time (1062 s) compared to the rest. The pulsar PSR J1748-2446ad with a frequency of 716 Hz is the fastest.

A rotating neutron star is composed of uniform matter of degenerate baryons in the core where neutrons and protons could be superfluid and superconducting respectively, surrounded by a crust made of nuclei and superfluid neutrons and is modeled by a stationary, axisymmetric, perfect fluid space-time. The presence of solid crust contributes to negligible departure (of the order of  $10^{-5}$ ) from perfect fluid equilibrium. Within the few years of formation, the interior temperature of a neutron star becomes  $\sim 10^9 K$ , that is negligible compared to the Fermi energy of the constituent dense matter. Hence, the effect of finite temperature is ignored. Also with time, the outer crust becomes superfluid and the nucleons form an array of vortices due to rotation. The characteristic length over which the gravitational field of the rotating star varies is much larger than distance between the vortices. So the relativistic star is modeled as a uniformly rotating, zero-temperature perfect fluid.<sup>25</sup>

As there is no analytical self-consistent solution for the space-time, several numerical codes are developed to study the rotating relativistic stars. We use rns code,<sup>26</sup> which constructs models of rapidly rotating, relativistic, compact stars using Komatsu, Eriguchi and Hachisu (KEH) scheme.<sup>27</sup> Here the field equations and the equation of hydrostatic equilibrium are solved iteratively by fixing the central energy density and any of the other variables such as mass, rest mass, angular velocity, angular momentum or the ratio of polar radius to the equatorial radius until convergence. We run the code for our tabulated, zero-temperature EoS, consisting of energy density, pressure, enthalpy and number density. The code also incorporates modifications by Cook, Shapiro and Teukolsky,<sup>28</sup> where a new radial variable is introduced that maps semi-infinite region to the closed region, unlike KEH scheme. In KEH scheme, the region of integration was truncated at a finite distance from the star.

A rotating star can support larger mass compared to a static one. In a rapidly rotating neutron star model, we can follow the quasi stationary evolution of a single star along the constant rest mass sequences. We have two equilibrium sequences

termed as "normal" and "supramassive". Normal sequences start rotating with Keplerian frequencies and end up on the static limit, which is stable to quasi-radial perturbation. On the other hand, the supra-massive sequence does not have a corresponding static solution. They have rest masses that are higher than their static (TOV) counterparts. We study these high mass stars in this work.

Recently, we adopted a density dependent relativistic mean field model where hyperons and antikaon condensates were considered apart from the nucleons and leptons.<sup>23</sup> In this model baryon-baryon interactions are mediated by  $\sigma$ ,  $\omega$  and  $\rho$  mesons. The salient feature of this model is the appearance of rearrangement term due to density dependent meson-baryon couplings which takes care of many body effects and the thermodynamic consistency<sup>29</sup> in dense neutron star matter. Nucleon-meson couplings of the model are determined from binding energies, spin-orbit splittings, charge and diffraction radii, surface thickness and neutron skin of finite nuclei following the DD2 model of Typel *et. al.*<sup>30,31</sup> Consequently, our model leads to symmetric nuclear matter properties at the saturation density for example binding energy per nucleon 16.02 MeV, incompressibility 243 MeV, symmetry energy 31.67 MeV and its slope parameter corresponding to the density dependence of symmetry energy 55.03 MeV. These values, particularly symmetry energy and its slope parameter are in excellent agreement with experimental findings.<sup>32</sup> The equation of state (EoS) in the sub-saturation density regime is well constrained. It should be noted that other density dependent parametrizations were extensively used in the calculation of neutron stars for example DDME2 parameter set.<sup>33</sup> It has been shown that nuclear matter properties at the saturation density and maximum neutron star mass calculated with DD2 and DDME2 sets are very similar.<sup>34</sup>

The density-dependent meson-hyperon couplings are obtained from the density dependent meson-nucleon couplings using hypernuclei data<sup>35</sup> and scaling law.<sup>36</sup> Analysis of hypernuclei events predict an attractive potential for  $\Lambda$  and  $\Xi$  and a repulsive potential for  $\Sigma$  in symmetric nuclear matter. We have considered  $\Lambda$ ,  $\Sigma$  and  $\Xi$  hyperons in this calculation and the scalar meson couplings to these hyperons are fitted to the experimental value of potential depth of respective hyperons ( $U_{\Lambda}^N(n_0) = -30$  MeV,  $U_{\Xi}^N(n_0) = -18$  MeV,  $U_{\Sigma}^N(n_0) = +30$  MeV) in saturated nuclear matter.<sup>23</sup> The repulsive interaction among the hyperons are also considered within the model, it is mediated by the exchange of  $\phi(1020)$  mesons. The couplings of antikaon-nucleon interactions are obtained similarly, however, they are not density-dependent. The particular choice of hyperon-nucleon potential does not affect the maximum mass of neutron stars,<sup>37</sup> but it varies with optical potential of (anti)kaons in nuclear matter.<sup>23</sup> Recently there have been studies of hypernuclear matter in neutron stars which meet the  $2M_{solar}$  mass limit.<sup>38,39</sup> The ref<sup>39</sup> gauges the parameters of the density-dependent functional with hypernuclei. There are several hyperon EoS which are reviewed in Ref.<sup>40</sup> Out of them presence of  $\Sigma^-$  for a repulsive potential is confirmed along with  $\Lambda$  and  $\Xi$  hyperons only in case of a few EoS models, i.e. BM165,<sup>41</sup> DS08,<sup>42</sup> UU1 and UU2.<sup>43</sup> However, only BM165 and DS08 are consistent with  $2M_{solar}$  observation.<sup>5-7</sup>

Our EoS including hyperon and antikaon condensed matter is consistent with the observational limit of  $2M_{solar}$ ,<sup>5-7</sup> unlike most of the existing exotic EoS. We restrict our comparison to hadronic EoS only. Furthermore, it is interesting to note that the pure neutron matter EoS calculated with DD2 set agrees well with the Chiral effective field theory result.<sup>44,45</sup>

### 3. Results

We report our results for rotating neutron star calculated using rns code<sup>26</sup> for our EoS. The fastest rotating pulsar observed until now has a frequency 716 Hz or angular velocity  $\Omega \approx 4500s^{-1}$ . Our choice of angular velocity ( $\Omega$ ) values (5300, 5800 & 6300 $s^{-1}$ ) are slightly more but of the same order of magnitude. The motivation of these choices are to study the effect of rapid rotation on the universal relations in case of millisecond or sub-millisecond pulsars. The different sets of EoS, Pressure ( $P$ ) versus energy density ( $\epsilon$ ), are plotted in Fig 1 and denoted by their respective compositions. In the Fig 1a, we plot the nucleons-only (np) EoS in red; neutron, proton,  $\Lambda$  (np $\Lambda$ ) EoS in blue; neutron, proton,  $\Lambda$ ,  $\Sigma^-$ ,  $\Xi^0$  (np $\Lambda\Sigma\Xi$ ) EoS in cyan; neutron, proton,  $\Lambda$ ,  $\Xi^0$ ,  $\Xi^-$  (np $\Lambda\Xi$ ) EoS in green and neutron, proton,  $\Lambda$ ,  $\Xi^0$ ,  $\Xi^-$ , antikaon condensates(np $\Lambda\Xi K$ ) EoS in maroon. These EoS are generated within the framework of DD2 model.<sup>23</sup> Presence of hyperon makes the EoS softer compared to nucleons-only case. For np $\Lambda$  EoS  $\Lambda$  appears at  $2.20n_0$ , for np $\Lambda\Sigma\Xi$  EoS  $\Sigma^-$  and  $\Xi^0$  appear at  $2.48n_0$  and  $6.26n_0$  respectively. Presence of  $\Sigma^-$  does not allow  $\Xi^-$  in the system. Finally for np $\Lambda\Xi$ ,  $\Xi^-$  and  $\Xi^0$  appear at  $2.44n_0$  and  $7.93n_0$  respectively.<sup>23</sup> The study of Kaonic atoms suggests an attractive optical potential for the (anti)kaons in nuclear matter. However, there is no definite consensus how deep the potential is. We report our results for a set of values of  $U_{\bar{K}}$  from -60 to -140 MeV in Fig 1b. These EoS are for neutron, proton and antikaon condensates (denoted by np $K$ ). The coupling constants for kaons with  $\sigma$ -meson,  $g_{\sigma K}$  at the saturation density for the range of  $U_{\bar{K}}$  for DD2 model are listed in Table 2 of Ref.<sup>23</sup> The deeper the antikaon potential in nuclear medium, softer is the EoS. In Fig 1a we also consider the presence of  $\Lambda$  and  $\Xi$  hyperons as well as the (anti)kaon condensates. Since early presence of hyperons delay the appearance of  $K^-$  condensates to higher density, effect of  $K^-$  condensates is only considerable for  $|U_{\bar{K}}| \geq 140$  MeV. So we consider neutron, proton,  $\Lambda$ ,  $\Xi$ , antikaon condensates (np $\Lambda\Xi K$ ) for  $U_{\bar{K}} = -140$  MeV only in Fig 1a.

In Fig 2a and 2b, we plot the gravitational mass as a function of equatorial radius for different compositions (np, np $\Lambda$ , np $\Lambda\Sigma\Xi$ , np $\Lambda\Xi$ , np $\Lambda\Xi K$ , denoted by red, blue, cyan, green and maroon respectively in the online version). The gravitational mass of neutron star for static sequence and the sequence rotating at their Kepler frequencies are represented by solid lines at the left and right extremes. The solid circles on these sequences indicate the maximum masses for the sequences. We have noticed in Fig 1a, the overall EoS is softer as we increase the degrees of freedom in the form of exotic particles. This leads to fall of maximum mass values from np to

np $\Lambda$  $\Xi$ K in both the static and mass shedding sequences. However, the corresponding radius does not change much with the composition.

The maximum mass and corresponding radius of the star with different composition for static and Kepler sequences are listed in Tables 1 and 2. We notice that a star rotating at its maximum possible frequency i.e. Kepler frequency, can support more mass compared to the static one. As the centrifugal force increases with the rotational velocity, the stars tend to have larger radii. For each set of EoS the maximum mass increases almost by 20% from static to Kepler. In between static and Kepler sequences, three fixed angular velocity sequences are plotted in Fig 2a for  $\Omega = 6300, 5800, \text{ and } 5300 \text{ s}^{-1}$  denoted by dotted, dashed and dash-dotted line respectively. The lines with different constituents but same frequency converge for relatively larger stars, whereas for smaller stars different frequency lines merge for same set of constituents. Or in other words, mass sequence of the small(large) rotating stars are dependent(independent) of EoS.

In between the static and Kepler limits, fixed rest mass curves are drawn in Fig 2b. The horizontal curves denoted by I, II, III and IV are for rest mass,  $M_R = 1.92, 2.49, 2.75 \text{ and } 3.23 M_{solar}$  respectively. All the lines in I, np (red) in II and III are normal sequence; np (red) in IV, np $\Lambda$ (blue), np $\Lambda$  $\Sigma$  $\Xi$ (cyan), np $\Lambda$  $\Xi$ (green) and np $\Lambda$  $\Xi$ K(maroon) lines in II and III are supramassive. The red dashed line marked as IV is for  $M_R = 3.23 M_{solar}$ . This value is well above the maximum mass for the exotic EoS, here we have a single sequence corresponding to np EoS only. Stars on the supramassive sequence may evolve keeping their rest mass constant but changing the spin rate. The stars on the supramassive sequences typically lose energy and angular momentum very slowly by emitting radiation. As they reach the point of quasi-radial instability, they rapidly spin up before collapsing into a black hole.<sup>46</sup>

We plot the critical masses i.e., the maximum masses(M) of the constant angular momentum(J) stellar models, such that  $(\partial M/\partial \rho_c)_J = 0$ , where  $\rho_c$  is the central density. Beyond this point the stellar models become unstable. The critical masses vary considerably when plotted with the angular momentum as seen in Fig 3a. Each sequence starts at  $M_{crit} = M_{static}$  where  $M_{static}$  is the maximum mass of a non-rotating sequence and ends at maximum angular momentum  $J = J_{Kepler}$  with  $M_{crit} = M_{Kepler}$ . They vary for different EoS. Larger mass of stellar configurations, for example np, supports higher Kepler frequency or angular momentum as can be seen from Fig 3a. However, the percentage change of stable mass configuration as the static star spins up to its Kepler limit is similar( $\sim 16 - 20\%$ ) for all the EoS. So we draw the same plots in Fig 3b, but in terms of dimensionless quantiles  $M_{crit}/M_{static}$  and normalised angular momentum where,  $j = J/M_{crit}^2$  and  $j_{Kepler} = J_{Kepler}/M_{Kepler}^2$ . We observe that the relation between normalized critical masses and normalized angular momentum does not vary much with the given equations of state. We find a universality (a 20% rise of  $M_{crit}$  value over  $M_{static}$  for all the EoS) in the normalised mass-angular momentum profile. We got a best-fit line  $M_{crit}/M_{static} = 1 + a_1x + a_2x^2 + a_3x^3$ , where  $x = j/j_{Kepler}$  and the coefficients are  $a_1 = 0.3363, a_2 = 0.3829, a_3 = 0.138$ . This treatment is particularly useful to

compute the maximum mass configuration allowed by uniform rotation in terms of its corresponding static sequence for all the EoS. Similar features have been reported in Ref<sup>21</sup> for nucleonic EoS, though their best fit parameters are slight different from ours. The dashed line with their parameters does not fit our data well at lower  $j/j_{kep}$ .

In Fig 4a we plot the variation of  $\mathbf{I}$  versus gravitational mass for EoS with different constituents at the Kepler frequency. For a neutron star of known mass and  $\mathbf{I}$ , we can deduce the radius using  $\mathbf{I}$  versus M and M versus R graphs. This eventually would help us constrain the EoS and confirm if the NS contains exotic core or not. In Fig 4a  $\mathbf{I}$  values are plotted for np, np $\Lambda$ , np $\Lambda\Sigma\Xi$ , np $\Lambda\Xi$  and np $\Lambda\Xi K$  ( $U_{\bar{K}} = -140$  MeV) as well as for np $K$ ;  $U_{\bar{K}}$  varies from -60 to -140 MeV. It is noted that  $\mathbf{I}$  is maximum for stiffer EoS, i.e. for np, it can support a heavier and more compact star. The maximum of  $\mathbf{I}$  curve however does not correspond to the maximum neutron star mass and the corresponding radius. The values of maximum  $\mathbf{I}$  and the corresponding masses, radii and angular velocity are listed in Tables 3 and 4. Currently, for PSRJ1614-2230, the lower limit of  $\mathbf{I}$  is estimated to be  $10^{45} g cm^2$  from  $\gamma$ -ray flux measurement.<sup>47</sup> This value is not very constraining due to uncertainty in the distance of the pulsar. The accuracy is expected to improve highly with the upcoming SKA results.

In Fig 4b,  $\mathbf{I}$  is plotted for different angular frequencies ( $\Omega=5300, 5800$  and  $6300 s^{-1}$ ). We have considered np, np $\Lambda$ , np $\Lambda\Sigma\Xi$ , np $\Lambda\Xi$  and np $\Lambda\Xi K$  EoS.  $\mathbf{I}$  is less for a star rotating at  $\Omega = 5300 s^{-1}$  compared to that of  $6300 s^{-1}$ .

The moment of inertia versus the angular velocity for all np, np $\Lambda$ , np $\Lambda\Sigma\Xi$ , np $\Lambda\Xi$  and np $\Lambda\Xi K$  cases are plotted in Fig 5a. Here also the same colour scheme is used for different compositions as in Fig 1. We find that  $\mathbf{I}$  is lower for softer EoS (np $\Lambda\Xi K$ ) compared to the stiffer ones (np, np $\Lambda$  etc) at a particular angular frequency. The four solid lines represent  $\mathbf{I}$  at Kepler frequency, each of those increase to a peak but falls for a relatively slower pulsar. For stiffest EoS, np,  $\mathbf{I}$  peaks at  $\Omega = 8740 s^{-1}$ , while the maximum occurs at  $\Omega = 7840 s^{-1}$ ,  $7660 s^{-1}$ ,  $7520 s^{-1}$ ,  $7510 s^{-1}$  for np $\Lambda$ , np $\Lambda\Sigma\Xi$ , np $\Lambda\Xi$  and np $\Lambda\Xi K$  ( $U_{\bar{K}} = -140 MeV$ ) respectively (See Table 3). We notice that the maximum angular velocity of rotating neutron stars is quite sensitive to the EoS. An EoS predicting smaller Keplerian frequencies than the observed frequencies can be ruled out and thus be useful in constraining EoS. We also plotted fixed rest mass  $M_R$  sequences in the same figure, which show different behaviour for different  $M_R$  and EoS. To understand the nature of moment of inertia curves in Fig 5a, we studied the variation of mass and radius terms with respect to angular frequency. We mention these results only qualitatively to analyse Fig 5a (not shown in separate graphs). For  $M_R = 1.92 M_{solar}$ , the sequences are found at lower  $\Omega$  region. Stars that are less massive can not sustain rapid rotation. We have noted both the mass and radius decrease monotonically at this angular frequency range, which explains the nature of  $\mathbf{I}$  curves. Also, The variation of  $\mathbf{I}$  with different compositions is negligible in this case. This is quite expected as we have found in horizontal curve I of Fig 2b that all EoS merge together for  $M_R = 1.92 M_{solar}$ . The central

energy density of a  $1.92M_{solar}$  static star differs from 7 to  $7.96 \times 10^{14}g/cm^3$  for np to  $np\Lambda\Xi K$ , whereas hyperons start populating at  $5.91 \times 10^{14}g/cm^3$ . The corresponding central density for a  $M_R = 1.92M_{solar}$  star rotating with Kepler frequency is only  $5.9 \times 10^{14}g/cm^3$ , so the effect of exotic particles is not there. The supra-massive star sequence  $M_R = 2.49M_{solar}$  also falls monotonically as  $\Omega$  decreases in case of all EoS(long dashed lines). However the monotonic fall is followed by a sudden spin-up with a slight loss of  $\mathbf{I}$  for this supra-massive sequence when the star contains exotic components. The nature of bending is different for different EoS and can be justified by following the variation of mass and radius with  $\Omega$ . Both of them decrease initially with decreasing  $\Omega$  to rebound at a particular angular frequency suddenly. Along a supra-massive sequence of a pulsar as  $\Omega$  decreases, a spin up followed by a second spin down after the initial one in the  $\mathbf{I}$  versus  $\Omega$  plane was reported in Ref.<sup>48-50</sup> This phenomenon is known as the back bending (S-shaped curve in the plot) and was attributed to the phase transition from nuclear matter to some exotic (hyperon, antikaon condensed or quark) matter. Interestingly, for the supra-massive sequence ( $M_R = 2.75M_{solar}$ , the dotted curves), value of  $\mathbf{I}$  falls off with higher angular velocity for the exotic EoS. However,  $M_R = 2.49$  as well  $2.75M_{solar}$ , corresponding to red long dashed and dotted lines, are normal sequences for np EoS and follow the same characteristic fall with decreasing  $\Omega$  like the normal sequences ( $M_R = 1.92M_{solar}$ ). Stars at normal sequences do not exhibit spin up even if they lose energy and angular momentum. This was also observed by Cook *et. al* in Ref.<sup>46</sup> The red dot dashed line is supramassive for np ( $M_R = 3.23M_{solar}$ ) and follows the same nature as the other exotic supramassive sequences with  $M_R = 2.75M_{solar}$ . For supramassive sequences, we also notice that the size of the star increases at low rotation speed. Though it can support a higher mass at higher rotation speed like the normal sequence, at low speed a higher mass star can be supported again. We show the variation of  $\Omega$  with the angular momentum  $J$  in Fig. 5b for the same sets of parameters as in Fig 5a. This helps us to check the stability of the rotating configurations.<sup>49</sup> The condition for instability along a constant rest mass sequence is  $\frac{dJ}{d\epsilon} \geq 0$ .<sup>14</sup> Supramassive sequences terminate at different values of  $\Omega$  below which the instability appears. It is found that angular momentum initially decreases with central energy density ( $\epsilon$ ). After the stable region, angular momentum (J) starts increasing with central energy density ( $\epsilon$ ). We notice the increase of J as the star spins up subsequently. This marks the instability in the configurations with respect to axisymmetric perturbations.

The dependence of  $\mathbf{I}/MR^2$  with compactness (M/R) is drawn in Fig 6a. It was shown by Lattimer and Schutz that other than very soft EoS, which gives a maximum mass of the order of  $1.6M_{solar}$ , a relatively unique relation existed between  $\mathbf{I}/MR^2$  and M/R.<sup>4</sup> We however note that though at lower compactness,  $\mathbf{I}/MR^2$  is independent of EoS, it clearly varies differently for different EoS at higher compactness; it is quite less for the soft EoS compared to nucleons-only EoS.  $\mathbf{I}/MR^2$  term on the other hand depends on angular velocity  $\Omega$  at lower compactness. It is

less for a star spinning at higher rotational speed. The dependence on  $\Omega$  is not that prominent at higher compactness. At this point we recall that all our EoS yields a maximum mass not less than  $2M_{solar}$  (See Tables 1, 2). Still we find deviation from universality at higher compactness for different constituents. We notice at low compactness, which is near Kepler frequency, the central energy density is such that hyperons or antikaons do not populate. So all the EoS are identical. Naturally here  $\mathbf{I}/MR^2$  is independent of EoS. However at higher compactness when the central energy density is high enough to populate exotic particles,  $\mathbf{I}/MR^2$  varies differently for different EoS. The deviation for a particular compactness (say 0.25-0.27) varies between 5-7% from np to np $\Lambda$  $\Xi$ K EoS. If we consider the highest Keplerian frequency, the difference between np and np $\Lambda$  $\Xi$ K EoS can be as high as 14%.

Similar trend is noticed for rapidly rotating stars from Fig 6b also:  $\mathbf{I}/MR^2$  for npK at different  $U_{\bar{K}}$ , is independent of EoS only at low compactness. The difference of  $\mathbf{I}/MR^2$  for softest and stiffest EoS at Keplerian frequency is  $\sim 7\%$ , whereas for a compactness 0.27, this varies around 2.5% as we change the optical potential of antikaons in nuclear matter from -60MeV to -140MeV. On an average these deviation from universality is of the same order as reported by Breu and Rezzolla for nucleonic EoS in Ref.<sup>21</sup>

We exhibit variation of moment of inertia in terms of another dimensionless quantity,  $\mathbf{I}/M^3$  with compactness for np, np $\Lambda$ , np $\Lambda$  $\Sigma$  $\Xi$ , np $\Lambda$  $\Xi$ , np $\Lambda$  $\Xi$ K in Fig 7a.<sup>21</sup> The three distinct bunches of lines differ in their angular velocity values  $\Omega$ , increasing from top to bottom. It is clearly seen that  $\mathbf{I}/M^3$  is also not affected by the different EoS and respects universality relation at lower compactness. However at higher compactness, a slight deviation from universality is evident. This part is zoomed in the inset. At a particular M/R value,  $\mathbf{I}/M^3$  drops considerably from np to np $\Lambda$  $\Xi$ K EoS.

In the next graph (Fig 7b) we look into the variation of  $\mathbf{I}/M^3$  with compactness for npK case. Here we consider different optical potential of antikaons  $U_{\bar{K}} = -60$  to  $-140$  MeV. The effect is similar as in Fig 6b. The variation of  $\mathbf{I}/M^3$  is dependent on  $\Omega$  values at lower compactness, it decreases for a faster rotating star. The variation with different composition i.e., EoS at higher compactness is clearly visible in the zoomed inset.

Finally in Fig 8, we show the variation of the normalised moment of inertia for the rest mass sequences I, II, III and IV of Fig 2b. Fixed rest mass sequence has also been used by Martinon et al.<sup>51</sup> to study quasistationary evolution of I-Love-Q universal relations for a particular EoS. In Fig 8a, we note  $\mathbf{I}/MR^2$  changes appreciably with EoS for supra-massive sequences, however is practically independent of EoS for normal sequence ( $1.92M_{solar}$  rest mass). The same pattern is noted for  $\mathbf{I}/M^3$  in Fig 8b. The anomalous behavior between the normal and supramassive sequences in Fig 8a and 8b, may be explained as the difference between the evolutionary track of an isolated star of sequences. While the normal sequence stars never spin up, the ones in the supramassive sequence spin up differently depending on their EoS. The universality is a signature of a balance between gravity and the response of matter

to gravity. These supramassive sequences seem to disrupt the balance.

#### 4. Discussion and Conclusion

Our main objective is to study the moment of inertia and different universal relations associated with it for a neutron star that has several exotic particles such as hyperons ( $\Lambda$ ,  $\Xi$ ,  $\Sigma$ ), (anti)kaon condensates in its high density core. We have constructed a set of EoS incorporating these exotic components individually as well as considering all of them together in the framework of a density dependent hadronic field theory using the DD2 parameter set. All our EoS satisfy the  $2M_{solar}$  observational constraint. The EoS of hyperon matter calculated using DDME2 set also resulted in  $2 M_{solar}$ .<sup>29,38</sup> We employ them to study the structure of rapidly rotating neutron stars. Also as the stars spin up, the maximum masses they can support go up and the stars become larger in size for all the EoS considered. In this connection, we consider the equilibrium mass of the star at maximum angular momentum, beyond which the configuration becomes unstable and call this mass as critical mass following Ref.<sup>21</sup> We find that though different equations of state give rise to different maximum masses and end up at different angular momenta, the maximum mass supported by rotation is almost 16-20% more than that supported by their corresponding static sequences for all the EoS. Hence we express this critical mass sequences of rapidly rotating stars in terms of the static mass solution and normalised angular momentum and show that a universal relation holds irrespective of the different constituents or EoS, the variation at Kepler limit being 20% larger than the static limit. This number is in full agreement with the results for nucleonic EoS by Breu and Rezzolla.<sup>21</sup>

Next we focus on moment of inertia for different compositions and explore its variation with mass. The larger the value of  $\mathbf{I}$ , the larger is the maximum mass supported by the stellar models, and more compact is the star. Also, stiffer EoS can withstand higher angular velocity. We came to these conclusions for the dense matter containing exotic degrees of freedom.

We followed the fixed rest mass sequences of stellar models, both normal and supramassive and studied the variation of  $\mathbf{I}$ . Along normal sequences,  $\mathbf{I}$  falls off monotonically as the stars spin down. However, for the supramassive cases, we notice sudden spin up of the stars following a spin down.  $\mathbf{I}$  drops drastically during the spin down, but the fall of  $\mathbf{I}$  is not so prominent during the subsequent spin up. This effect was maximal in the np $\Lambda$  case. Next, we study the universal relations for normalised  $\mathbf{I}$ . They are very useful tools in astrophysics. With the upcoming SKA telescope, measurement of  $\mathbf{I}$  may be accomplished soon, which will help constraining the EoS. However, it is incredibly difficult because of a few things. First of all, there are very few relativistic binaries where the effect of  $\mathbf{I}$  on the periastron advance at 2PN can be observed. Then, in addition to periastron advance, at least two other post-Keplerian parameters are needed to be measured precisely. Even if the effect of spin orbit coupling is strong enough, we need to accumulate data of periastron advance

for a minimum 20% time of the precision period of the pulsar to get a minimum accuracy of 10% in the moment of inertia measurement. The precision period of one of the most suitable candidates for this measurement, PSR J0737-3039, is 75 years. Hence, both mass and  $I$  measurements are needed to be combined with the universal relations to get more accurate estimation of the radius as emphasized also by Breu and Rezzolla.<sup>21</sup> That is why it is vitally important to know if universality relations hold for the equations of state with considerable softening at higher densities in the presence of hyperons and antikaon condensates etc.

Therefore, we have studied the variation of normalised  $I$  with respect to compactness ( $M/R$ ) for all the constituents np, np $\Lambda$ , np $\Lambda\Sigma\Xi$ , np $\Lambda\Xi$ , np $\Lambda\Xi K$  ( $U_{\bar{K}} = -140$  MeV) and np $K$  ( $U_{\bar{K}} = -60$  to  $-140$  MeV).  $I$  is normalised with respect to  $MR^2$  as well as  $M^3$ . We report a 10% deviation on an average from universality at higher compactness for all the equations of state. However at lower compactness, the normalised  $I$  is independent of our choice of composition, only vary with angular velocity. We have also investigated the normalised  $I$  vs compactness relations for fixed rest mass sequences. The variation is quite large for supramassive sequences, while practically insensitive for the normal sequences. Thus, we conclude that except from the supramassive sequence stars, the universality relations holds true for a normal star with exotic components, as the deviation from universality is of the same order for stars with only nucleonic EoS previously reported.

## 5. Acknowledgement

S. S. Lenka would like to acknowledge the support of DST, India through INSPIRE fellowship. The authors are also thankful to Debades Bandyopadhyay for carefully reading the manuscript.

## References

1. R. N. Manchester, G.B. Hobbs, A. Teoh and M. Hobbs, *Astronomical. J.* **129** (2005) 1993-2006.  
<http://www.atnf.csiro.au/people/pulsar/psrcat/>
2. A. Watts et. al, arXiv:1501.00042, *Proceedings of Advancing Astrophysics with the Square Kilometre Array (AASKA14)*. (2014) 8-13 June.
3. S. Bhattacharyya, *Advances in Space Research* **45** (2010) 949-978.
4. J. M. Lattimer and B. F. Schutz, *Astrophys. J.* **629** (2005) 979.
5. P.B. Demorest, T. Pennucci, S.M. Ransom, M.S.E. Roberts, J.W.T. Hessels, *Nature* **467** (2010) 1081-1083.
6. J. Antoniadis, P. C. C. Freire, N. Wex, T. M. Tauris et al., *Science* **340** (2013) 448.
7. E. Fonseca et. al, *Astrophys. J* **832** (2016) 167.
8. T. Damour and G. Schafer, *Nuovo Cimento B Series* **101** (1988) 127-176.
9. Y. Shao and X-D Li, *Astrophys. J* **816** (2016) 45.
10. M. Kramer and N. Wex, *Classical and Quantum Gravity* **26** (2009) 073001.
11. P. Haensel, M. Bejger, M. Fortin, L. Zdunik, *Eur. Phys. J. A* **52** (2016) 1-21 Art ID 59. and references therein.
12. N.K. Glendenning, S. Pei and F. Weber, *Phy. Rev. Let.* **79** (1997) 1603.

- 14 *S.S.Lenka, P.Char, S. Banik*
13. J.L. Zdunik, M. Bejger, P. Haensel and E. Gourgoulhon, *Astron. Astrophys.* **450** (2006) 747-758.
  14. N.K. Glendenning, *Compact stars Springer* New York (1997).
  15. K. Yagi and N. Yunes, *Science* **341** (2013) 365-368.
  16. K. Yagi and N. Yunes, *Phys. Rev.* **D88** (2013) 023009 .
  17. D. D. Doneva, S. S. Yazadjiev, N. Stergioulas, and K. D. Kokkotas, *Astrophys. J.* **781** (2014) L6.
  18. B. Haskell, R. Ciolfi, F. Pannarale, and L. Rezzolla, *Mon. Not. R. Astron. Soc. Lett.* **438** (2014) L71-L75.
  19. D. G. Ravenhall and C. J. Pethick, *Astrophys. J.* **424** (1994) 846-851.
  20. J. M. Lattimer and M. Prakash, *Astrophys. J.* **550** (2001) 426.
  21. C. Breu and L. Rezzolla, *MNRAS* **459** (2016) 646-656.
  22. S. Chakrabarti, T. Delsate, N. Grlebeck, and J. Steinhoff, *Phys. Rev. Lett.* **112** (2014) 201102.
  23. P. Char and S. Banik, *Phys. Rev.* **C90** (2014) 015801.
  24. S. Banik and D. Bandyopadhyay, *Phys. Rev.* **C66** 065801 (2002).
  25. J. Friedman, N. Stergioulas, *Rotating Relativistic Stars* Cambridge Univ Press 2013.
  26. N. Stergioulas and J. L. Friedman, *Astrophys. J.* **444** (1995) 306.
  27. H. Komatsu, Y. Eriguchi, I. Hachisu, *MNRAS* **237** (1989) 355-379.
  28. G. B. Cook, S. L. Shapiro, S. A. Teukolsky, *Astrophys. J.* **422** (1994) 227-242.
  29. G. Colucci and A. Sedrakian, *Phys. Rev.* **C 87**, 055806 (2013).
  30. S. Typel, *Phys. Rev.* **C71** (2005) 064301.
  31. S. Typel, G. Röpke, T. Klähn, D. Blaschke and H.H. Wolter, *Phys. Rev.* **C 81** (2010) 015803.
  32. J. M. Lattimer and Y. Lim, *Astrophys. J.* **771** (2013) 51.
  33. G. A. Lalazissis, T. Niksic, D. Vretenar and P. Ring, *Phy. Rev.* **C 71**, 024312 (2005).
  34. M. Fortin et al., *Phy Rev* **C 94**, 035804 (2016).
  35. J. Schaffner and I.N. Mishustin, *Phys. Rev.* **C53** (1996) 1416.
  36. C.M. Keil, F. Hofmann and H. Lenske, *Phys. Rev.* **C61** (2000) 064309.
  37. S. Weissenborn, D. Chatterjee, and J. Schaffner-Bielich, *Nucl. Phys. A* **881** (2012) 62-77.
  38. E.N. E. van Dalen, G. Colucci, A. Sedrakian, *Phys. Lett.* **B 734** 383-387 (2014).
  39. L. Tolos, M. Centelles and Angels Ramos, *Astrophys. J* **834** 3 (2017).
  40. M. Fortin, J.L.Zdunik, P. Haensel, M. Bejger, *A & A* **576** (2015) A68.
  41. I. Bednarek, P.Haensel, J.L. Zdunik, M. Bejger, R. Manka, *A & A* **543** (2012) A157.
  42. V. Dexheimer, S. Schramm, *Astrophys. J.* **683** (2008) 943.
  43. S. T. Uechi, H. Uechi, *Advances in High Energy Physics* Hindavi Publishing Corporation 2009 (2009) Art ID 640919.
  44. T. Fischer et al., *Eur. Phys. J.* **A50** (2014) 46.
  45. M. Oertel, M. Hempel, T. Klähn, S. Typel *Rev. Mod. Phys.* **89** (2017) 015007.
  46. B. G. Cook, S. L. Shapiro, S. A. Teukolsky, *Astrophys. J. Part 1* **424** (1994) 823-845.
  47. A. A. Abdo, M. Ackermann et al., *Science* **325** (2009) 840-844.
  48. F. Weber, ed, *Pulsars as astrophysical laboratories for nuclear and particle physics* CRC press (1999).
  49. J. L. Zdunik, P. Haensel, E. Gourgoulhon, M. Bejger, *A & A.* **416** (2004) 1013-1022.
  50. S. Banik, M. Hanauske, D. Bandyopadhyay, W. Greiner, *Phys. Rev.* **D70** (2004) 123004.
  51. G. Martinon, A. Maselli, L. Gualtieri, and V. Ferrari, *Phys. Rev.* **D90** (2014) 064026.

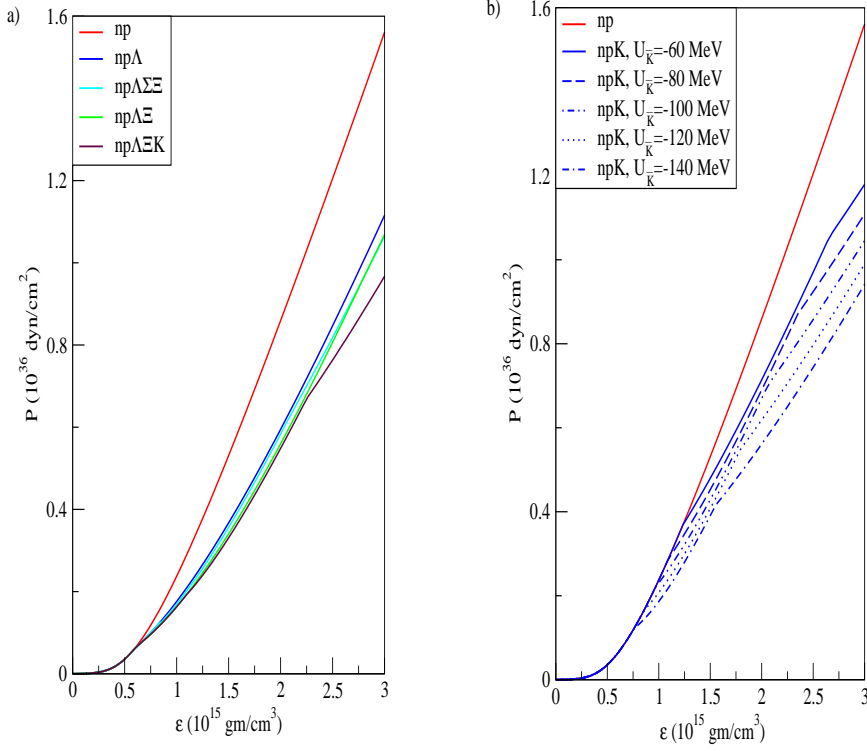


Fig. 1. Equation of state (EoS) for different compositions: a) np=red, np $\Lambda$ =blue, np $\Lambda\Sigma\Xi$ =cyan, np $\Lambda\Xi$ =green, np $\Lambda\Xi K$ =maroon colour in online version. b) np and npK for different  $U_{\bar{K}} = -60$  to  $-140$  MeV.

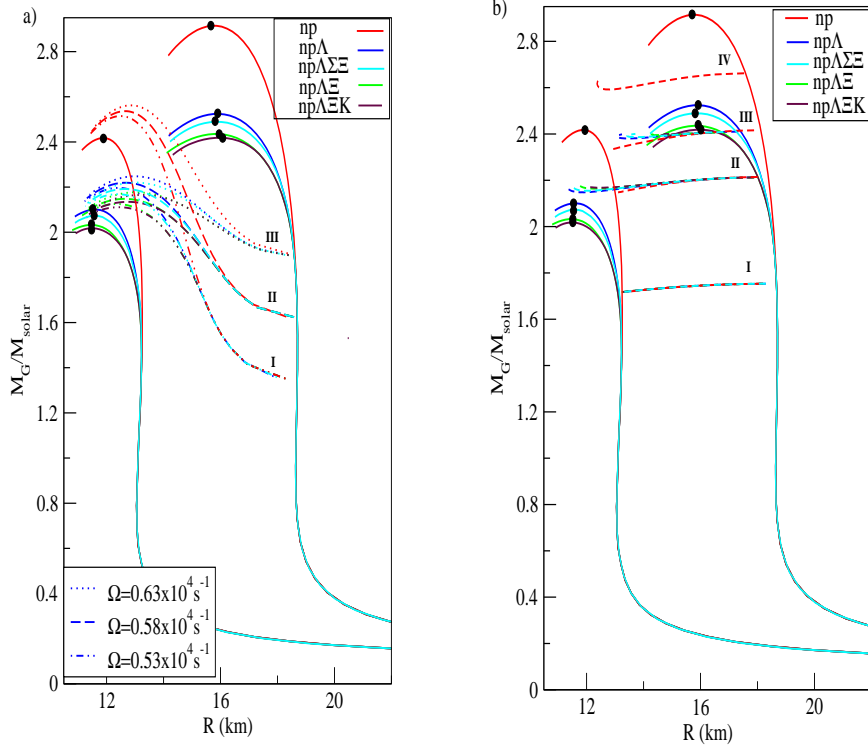


Fig. 2. Mass-radius profile for different compositions: np=red, np $\Lambda$ =blue, np $\Lambda\Sigma\xi$ =cyan, np $\Lambda\xi$ =green, np $\Lambda\xi K$ =maroon colour in online version. Static and Kepler mass-radius profiles are represented by solid lines on left and right extreme respectively. In between static and Kepler sequences are a) different fixed angular frequency curves I, II and III for  $\Omega=5300, 5800$  and  $6300 \text{ s}^{-1}$  respectively. b) different rest mass curves I, II, III and IV for rest mass  $M_R=1.92, 2.49, 2.75,$  and  $3.23 M_{solar}$  respectively.

Table 1. Maximum mass (in  $M_{solar}$ ) and the corresponding radius (in km) of compact stars with nucleons, hyperons and (anti)kaons in DD2 model.  $U_{\bar{K}} = -140 \text{ MeV}$  for np $\Lambda\xi K$  matter. The values in the parentheses are for the Kepler sequences.

	$M_{static[Kepler]} (M_{solar})$ ( $M_{solar}$ )	$R_{static[Kepler]} (\text{Km})$ (Km)
np	2.42[2.91]	11.91[15.68]
np $\Lambda$	2.10[2.52]	11.55[15.94]
np $\Lambda\Sigma\xi$	2.07[2.48]	11.56[15.82]
np $\Lambda\xi$	2.03[2.43]	11.49[15.97]
np $\Lambda\xi K$	2.01[2.41]	11.49[16.02]

Table 2. Maximum mass (in  $M_{solar}$ ) and the corresponding radius(in km) of compact stars with nucleons and (anti)kaons for different values of optical potential depth in the DD2 model. The values in the parentheses are for the Kepler sequences.

$U_{\bar{K}}$ (MeV)	$M_{static[Kepler]}$ ( $M_{solar}$ )	$R_{static[Kepler]}$ (Km)
-60	2.37[2.88]	12.19[16.10]
-80	2.34[2.85]	12.20[16.38]
-100	2.29[2.80]	12.18[16.45]
-120	2.24[2.72]	12.05[16.47]
-140	2.16[2.62]	12.03[16.27]

Table 3. Maximum moment of inertia and corresponding masses, radii and angular velocity of compact stars with nucleons, hyperons and (anti)kaons in the DD2 model.  $I$  is in  $10^{45} g cm^2$ , maximum mass is in  $M_{solar}$ , radius in km and rotational velocity  $\Omega$  in  $10^4 s^{-1}$ ,  $U_{\bar{K}} = -140$  MeV for  $np\Lambda\Sigma K$  matter.

	$I$ ( $10^{45} g cm^2$ )	M ( $M_{solar}$ )	R (Km)	$\Omega$ ( $10^4 s^{-1}$ )
np	5.70	2.84	16.8	0.874
np $\Lambda$	4.53	2.43	17.2	0.784
np $\Lambda\Sigma\Xi$	4.45	2.38	17.4	0.766
np $\Lambda\Xi$	4.30	2.32	17.5	0.752
np $\Lambda\Xi K$	4.30	2.32	17.5	0.751

Table 4. Maximum moment of inertia and corresponding masses, radii and angular velocity of compact stars with nucleons and (anti)kaons for different values of optical potential depth in the DD2 model.  $I$  is in  $10^{45} g cm^2$ , maximum mass is in  $M_{solar}$ , radius in km and rotational velocity  $\Omega$  at  $10^4 s^{-1}$ .

	$I$ ( $10^{45} g cm^2$ )	M ( $M_{solar}$ )	R (Km)	$\Omega$ ( $10^4 s^{-1}$ )
-60	5.70	2.84	16.8	0.874
-80	5.68	2.81	16.94	0.860
-100	5.59	2.74	17.22	0.832
-120	5.37	2.67	17.33	0.814
-140	5.01	2.53	17.5	0.780

18 *S.S.Lenka, P.Char, S. Banik*

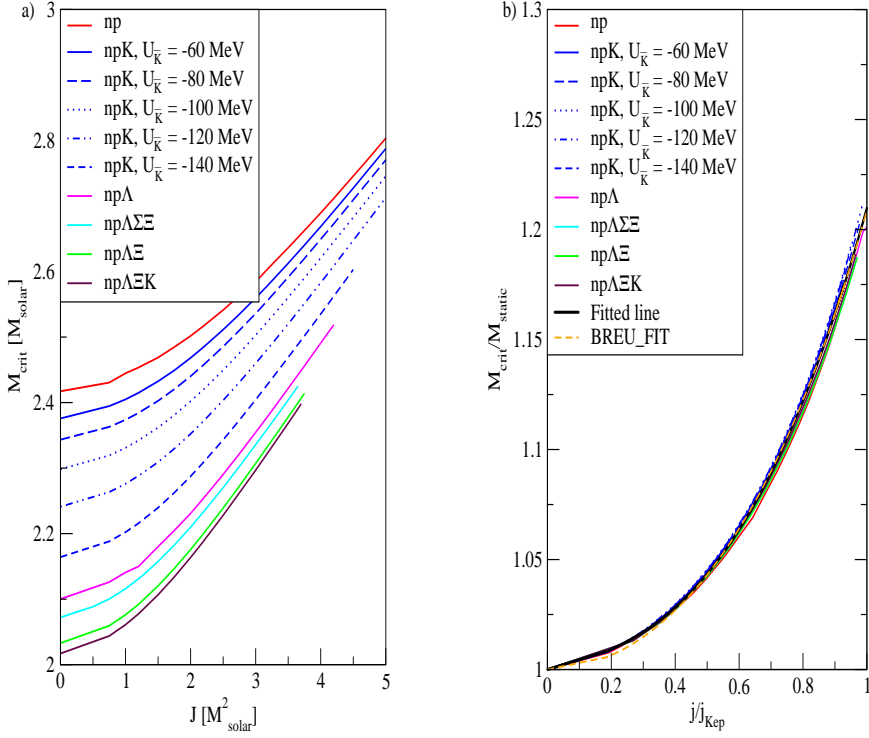


Fig. 3. a) Critical mass i.e. the maximum mass of the constant angular momentum stellar model versus the corresponding fixed angular momentum b) Normalised critical mass ( $M_{crit}/M_{static}$ ) versus normalised angular momentum.

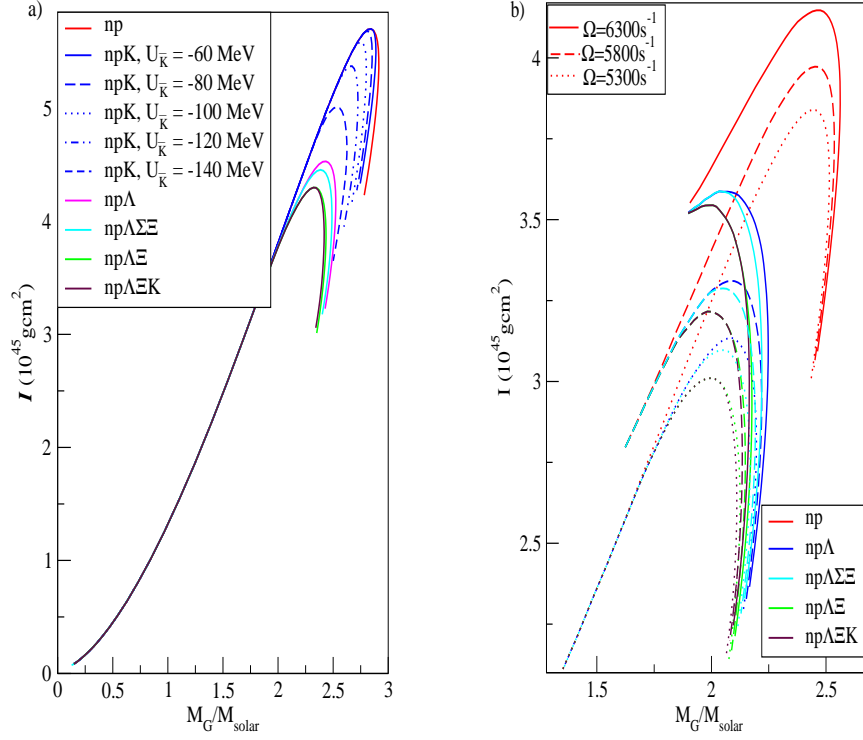


Fig. 4. Moment of inertia( $I$ ) versus gravitational mass( $M_G$ ) for different compositions of the neutron stars rotating a)at Kepler frequency b)at different angular frequencies.

20 *S.S.Lenka, P.Char, S. Banik*

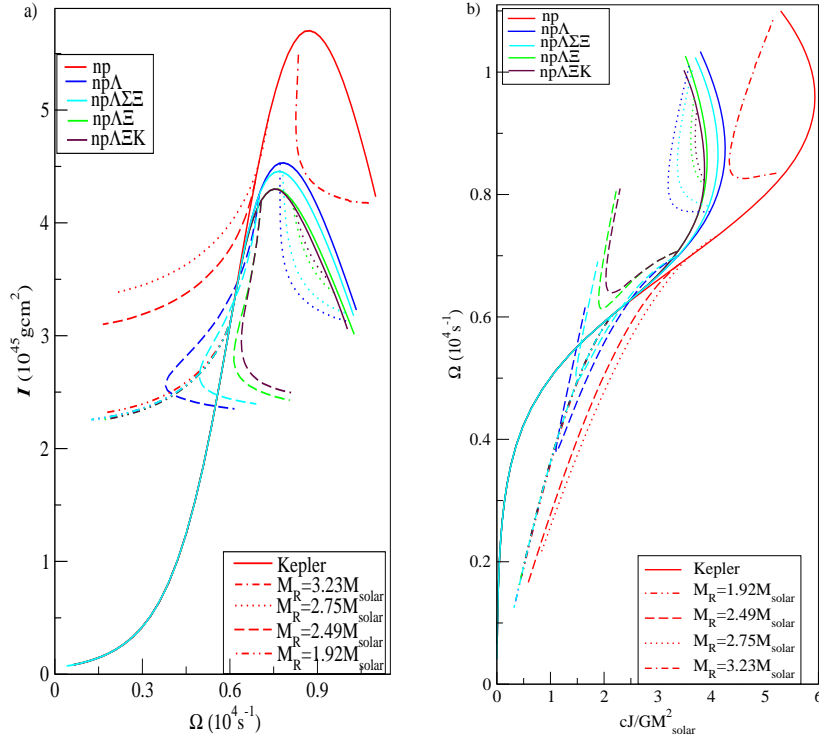


Fig. 5. a) Moment of inertia ( $I$ ) versus angular velocity ( $\Omega$ ). b) Angular velocity ( $\Omega$ ) versus angular momentum ( $cJ/GM_{\text{solar}}^2$ ). The solid lines correspond to Kepler frequency. Others are for different fixed rest mass sequences.

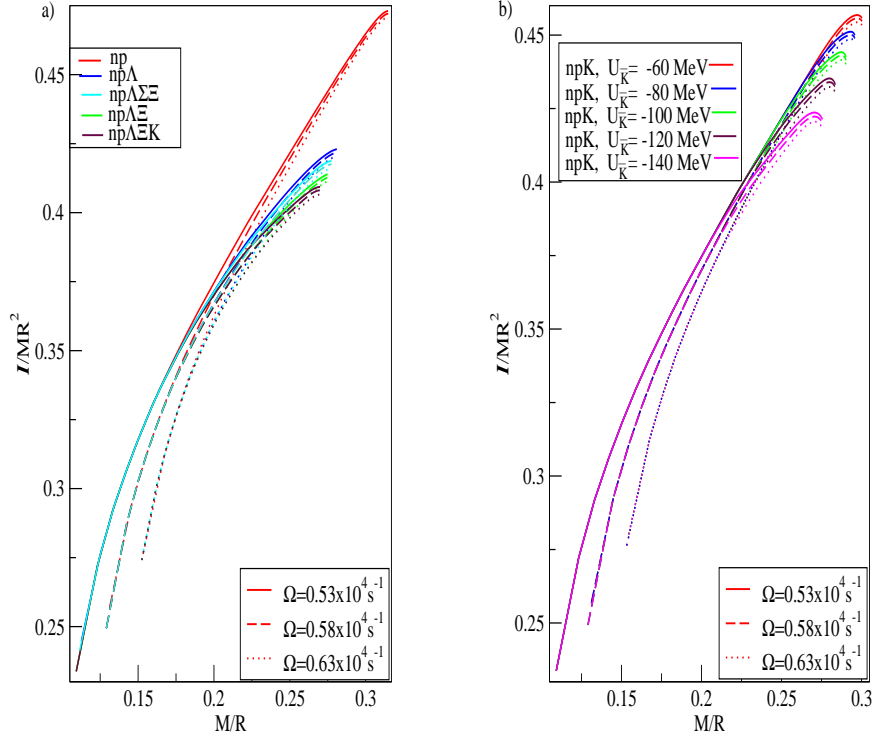


Fig. 6. Normalised moment of inertia( $I/MR^2$ ) with compactness for a)np, np $\Lambda$ , np $\Lambda\Sigma\xi$ , np $\Lambda\xi$ , np $\Lambda\xi K$ ,  $U_{\bar{K}} = -140 \text{ MeV}$  b)npK with different  $U_{\bar{K}}$

22 *S.S.Lenka, P.Char, S. Banik*

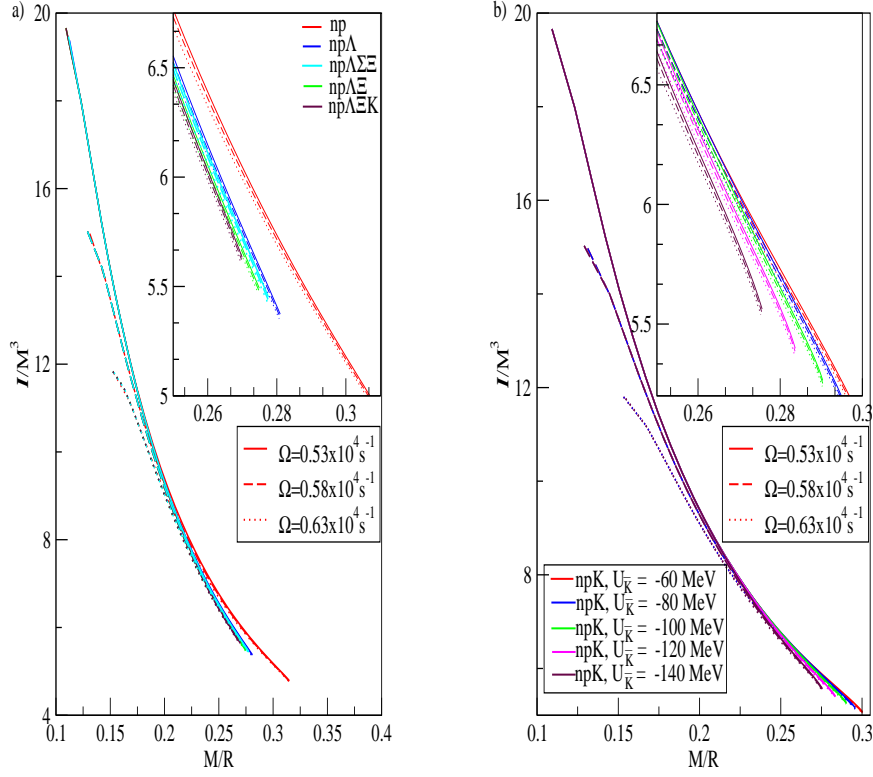


Fig. 7. Normalised moment of inertia( $I/M^3$ ) with compactness for a)np,  $np\Lambda$ ,  $np\Lambda\Sigma\Xi$ ,  $np\Lambda\Xi$ ,  $np\Lambda\Xi K$ ,  $U_{\bar{K}} = -140\text{MeV}$  b)  $npK$  with different  $U_{\bar{K}}$

*Critical mass, moment of inertia and universal relations of rapidly rotating neutron stars with exotic matter* 23

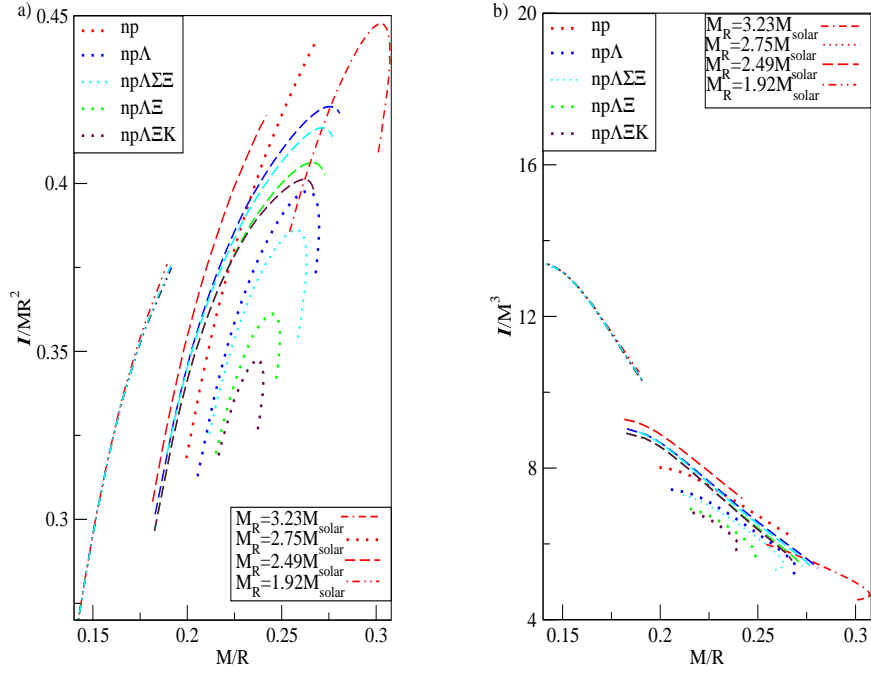


Fig. 8. Normalised moment of inertia as a function of compactness  $M/R$  a)  $I/MR^2$  versus  $M/R$  b)  $I/M^3$  versus  $M/R$  for the rest mass sequences  $M_R = 1.92, 2.49, 2.75$  and  $3.23 M_{\text{solar}}$ .